D0-note/3398

Januaryx 1998

Results from a Beam Test of the Forward Preshower Detector for the DØupgrade

Mrinmoy Bhattacharjee **Arnaud Lucotte**

State University of New York at Stony Brook

Abstract

Four modules of the Forward Preshower (FPS) detector were tested for the first time in a beam test during the summer of 1997. As the FPS detector is intended to enhance electron identification capability at the upgraded Tevatron, both a determination of the electron signature and the absolute calibration of the detector were needed.

This document reviews the analyses performed on the Beam Test data: in **section 1** the configuration of the FPS modules prepared for the test is presented. The signal routing from the detector to the front end electronic readout system is also briefly summarized. In **section 2**, electron selection is detailed: usually electrons are signaled by a deposition of energy shower behind the $2X_o$ thick lead converter, which is spatially matched with a hit consistent with a Mimimum Ionizing track (MIP) in the layers in front. In **section 3**, electron's signature is characterized for 50 and 70 GeV beams. Shower profiles as well as the beam energy dependence of the results are described. In **section 4**, data and Monte Carlo events are compared. As both samples are normalized independently, this comparison constitues a reliable test of the FPS simulation.

In the layers in front of the lead converter, charged pions tend to deposit a MIP. Taking advantage of high statistics samples, we used pions to measure the corresponding amount of collected charge. This procedure, which provides an absolute calibration for the detector, is reported in **section 5**.

Along with these analyses, the presence of a high level of electronic noise in the readout channels led to the development of efficient pedestal subtraction techniques. Based on a precise determination of the coherent part of the noise, these methods are reviewed in the appendix.

Contents

List of Figures

1 The FPS detector test bench

1.1 Module configuration

The final design of the Forward Preshower detector for DØis extensively detailed in [2]. It is intended to be mounted on the inner faces of the calorimeter endcaps for run II.
On each side, it consists of four layers of scintillator strips composed of sixteen 22.5^0 modules in ϕ. Each module consists of two layers of nested triangular (6.5mm -wide and 6mm -height) strips, forming a stereo angle of 22.5^0 with respect to one another. The two stereo (u and v) strips are perpendicular to either edge of a module. A $2X_0$ lead sheet separates the two small modules from the larger modules used to measure the shower energy.

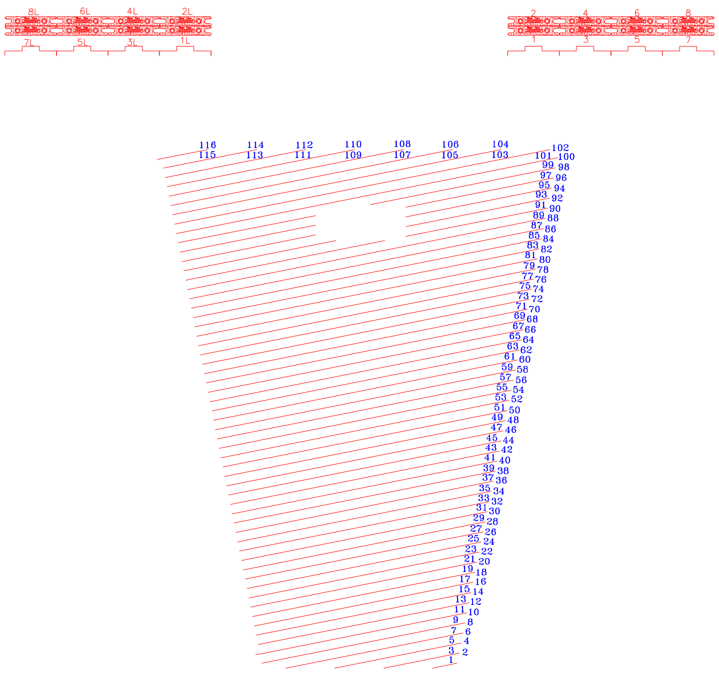

Figure 1.1: **Layout of a small module located in front of the $2X_0$ lead sheet**

A general layout of a small module used for the beam test is shown in Fig. 1.1. Two such small and two large modules were prepared for testing. 32 scintillator strips per modules were connected to the readout system, for a total of $4 \times 32 = 128$ channels. The active region equipped with readout cables spans about $32 \times 6.1 = 19.5$ cm of each module. Because of time constaints, only 2 modules were tested during the beam runs.

The modules were mounted on a moving table fitted with a mechanical system which enables one to move the detector in the upward/downward direction, as well as to rotate the detector in $\theta_{\rm det}$. The settings were fixed at a height h = $49\frac{3}{4}$ inches and an angle $\theta_{\rm det} = 6^0$ in order to simulate a $\theta = 15^0$ ($\eta = 2.01$) of incoming particles coming from the interaction point of the D0 detector, as sketched in Fig. 1.2.

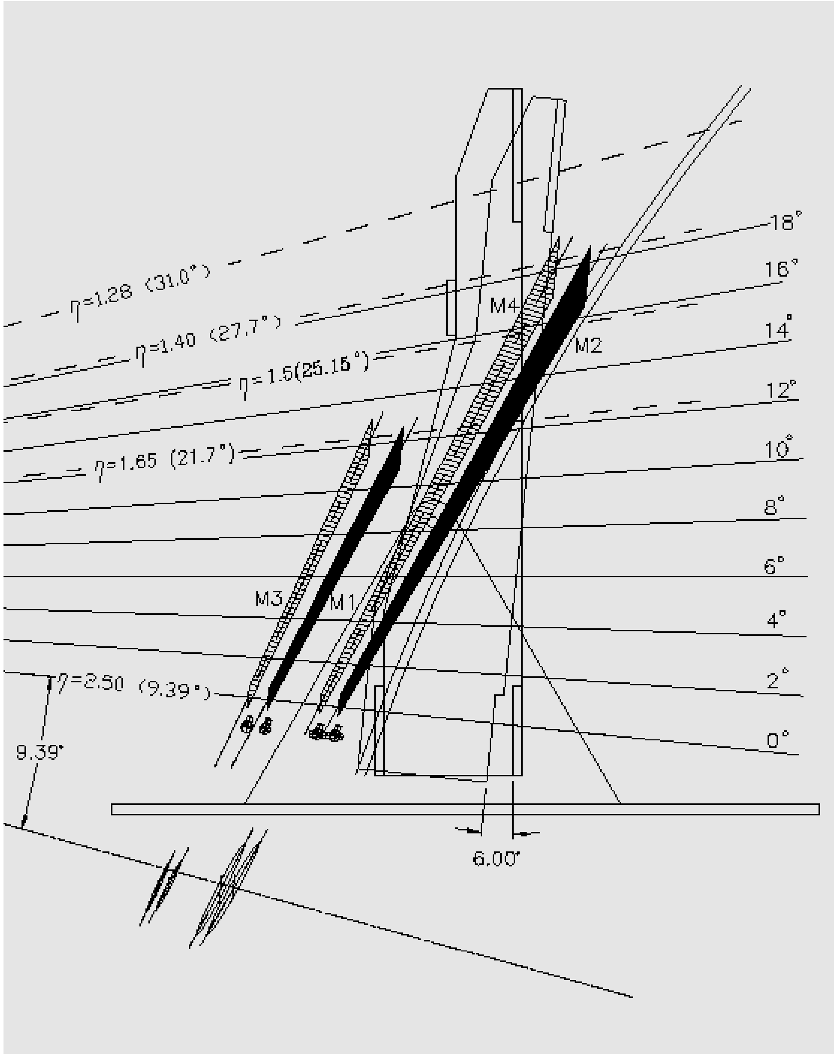

Figure 1.2: **Orientation in the transverse plane of the four modules during the Test beam**

1.2 Signal routing

A central hole in each triangular strip accomodates a Wave Lenght Shifting (WLS) fiber routed to the edge of the module, where connectors couple them to clear transmission fibers. These fibers were then brought around the module and routed down to HISTE IV Visible Light Photon Counter (VLPC) cassettes, where the light is converted to an electrical signal. These are arsenic doped silicon diodes that operate at a temperature of 6.5K with a bias of 6.5V. VLPC's are used for their high quantum efficiency, high gain with low dispersion and high signal forming speed with low noise. One VLPC cassette with 128 channels in total was used in the test beam. A charge division of the amount of charge going out from the VLPC as well as the dynamical range for each HISTE IV chip can be set. This defines the conversion factor between readout charge and MeV. Table 2 in **Appendix A** reports these specifications and charge division (within parentheses) for data and pedestal runs recorded during the Test Beam.

1.3 The Dataset

The test beam data have been divided into two periods, according to the configuration and equipped region of the FPS detector, as well as depending on the nature and energy of the beam. Throughout the rest of this note, the various part of the dataset will be referred to using names specified in Table 1.

During the first period, only the front two layers were equipped with output cables. Exposed to pion beam, the data analysis is devoted to the calibration of the detector using the MIP signal deposited in the layer infront of the lead converter.

In the second period, all four layers (two in front and two behind the lead converter) were read out. The detector was exposed alternatively to electron and pion beams. The collected data allowed for the characterization of the electron shower as well as abetter detector calibration due to increased statistics. During electron runs, a scan in beam energy has also been perfomed at 30, 50 and 70 GeV and was aimed at characterization of energy-dependence of the electron shower.

	Energy (GeV)	Name Electrons	Pions	Pedestal
Period 1	125 GeV		5,000	6,000
	30 GeV	5,500	7,200	50,000
Period 2	50 GeV	3,150	7,200	50,000
	70 GeV	11,000	7,200	50,000
	125 GeV		70,500	

Table 1: Statistics used for the two data taking periods.

1. **Period 1: Run 1057 to 1063** The two front layers were equiped with output cables, allowing 32×2 channels to be readout through the chips A0 and A1 for the U-layer and E0 and E1 for the V-layer.

   During this period, pions were targetted on the detector via a finger counter trigger, thus defining a 2-strips wide region actually hit by the particles. Data were collected with two different settings of the detector: the first set of runs (1057 to 1060) has been taken with the FPS at a fixed height of $49\frac{3}{4}$ inches, whereas runs 1061 to 1063 were taken after an 1/2 inch shift in the upward direction. The overall statistics accumulated during this period corresponds to about $5,000$ pions. The dynamical range for all chips was set at 100 fC.

2. **Period 2: Run 3000 to 4187** All the four layers were equipped with VLPC readout, corresponding to 32×4 channels readout via 8 chips, whose dynamical range settings were varied from run to run as reported in Table 2 in **appendix A**. Chips F2 and F3 were used for the front U layer and 92 and 93 for the front V. For the layers behind the lead, chips E0 and E1 were used for the U and A0 and A1 for the V layer.

   Electron and pion beams were used, and runs were peformed at 30 GeV, 50 GeV and 70 GeV for the electrons. The energy of the pion beam during this period was 125 GeV.

   However, it should be noted that finger counters were not used for these runs resulting in a wider 3.5×3.5 inches region of the detector being hit by the particles. This large spot size prevented from any a-priori determination of the fired channels.

2 Electron selection

Four modules of the detector have been exposed to 30, 50 and 70 GeV electron beams. The absence of the finger counter during these runs have resulted in a wider spread in the region of the detector hit by the beam preventing us from any a priori determination of hit channels. Figure 2.3 shows a typical sample of events taken during the electron runs. Almost 99.5% of the triggers turned out to be fakes. The analysis has thus been performed on an event by event basis, using a stringent and reliable electron selection algorithm. An algorithm has been developed to identify electrons.

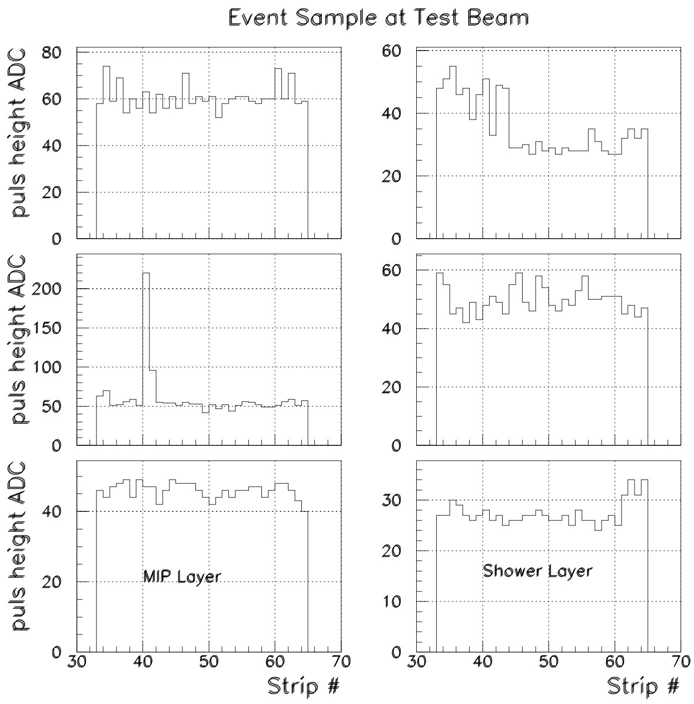

Figure 2.3: **A sample of events taken during the electron runs. Figures on left show signal in MIP layers while right hand shows signal in shower layers in three different events typical of this running period.**

2.1 Selection algorithm

An electron should leave a minimum ionizing track in the layers of scintillator in front of the lead converter spatially matched by a shower behind. As the FPS uses triangular strips, a MIP track will typically leave a signal only in two adjacent strips (nested pair) in the front layers.

The top plot of Fig. 2.4 shows the separation of strips with maximum and second maximum energy deposition in one of the front layers. As can be seen, this separation can be as large as 20-30 strips, and these can definitely be not electrons. Our signal is concentrated in the region where this separation is just one strip indicating that a particle has traversed two adjacent strips.

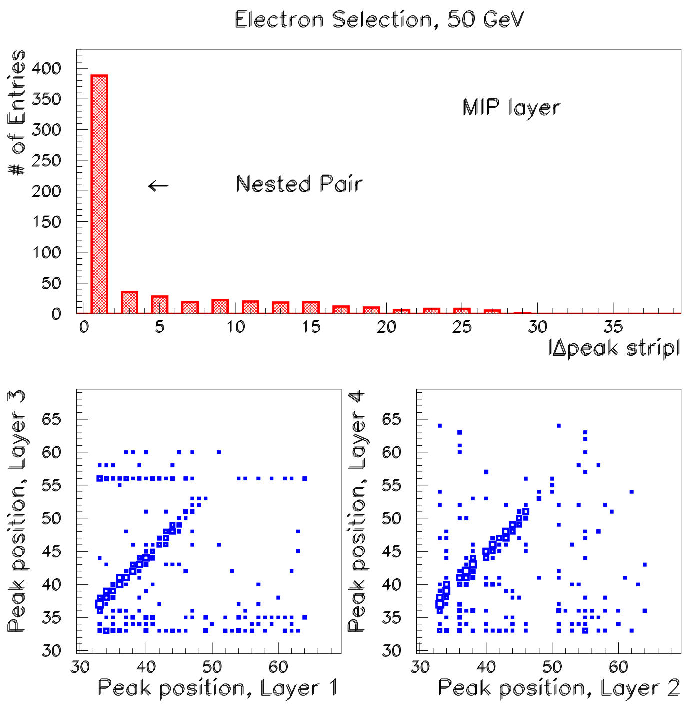

Figure 2.4: **Top figure shows signal in a nested pair of strips. The bottom two plots show the coincidence in signal between Layer 1 and 3 and Layer 2 and 4.**

Also, one should observe a coincidence in signal between front and rear layers when an electron passes through the detector. The bottom two plots of Fig. 2.4 shows the correlation in the peak position in Layer 1 (Layer 2) with the peak in Layer 3 (Layer 4). A narrow coincidence in peak position can be seen from these plots. This coincidence can be seen between other pairs of layers too, but since Layer 1 has strips going in the same direction as Layer 3 (both U layers) and similarly for Layer 2 and 4 (both V layers), the coincidence is narrowest for this combination. One can also see a systematic shift in the peak position towards higher strip number as we go from front to back layers. This can be understood from the fact that the beam hits the detector at an angle and hence it hits the rear layer at a higher strip index with respect to the hit position in the front layer. It can be seen from the figure that the hit position in Layer 3 (Layer 4) is at least 2 strips higher than that in Layer 1 (Layer 2). Based upon these observations the following electron selection algorithm was built.

- pulse height > 1 ADC count.
- all 8 chips should be readout properly (to ensure electronic stability during data taking).
- hot channels removed (pulse height > 255 ADC counts during the run)
- peak in each layer > 3σ of pedestal.
- only two adjacent strips are hit in the MIP layer (also ensures a clean MIP signal).
- front and rear coincidence defined as:
  2 strips $\leq$ peak(Layer 3)-peak(Layer 1) $\leq$ 8 strips.
  2 strips $\leq$ peak(Layer 4)-peak(Layer 2) $\leq$ 8 strips.

2.2 The pedestal subtraction

Pedestal runs were taken during the data taking. In the shower layers, the mean pedestal had a typical value of 20 ADC counts with a width of 15 counts, as seen in Fig. 2.7 and 2.8. Pedestal subtraction in the electron runs have been done using **method 3** defined in **Appendix B**.

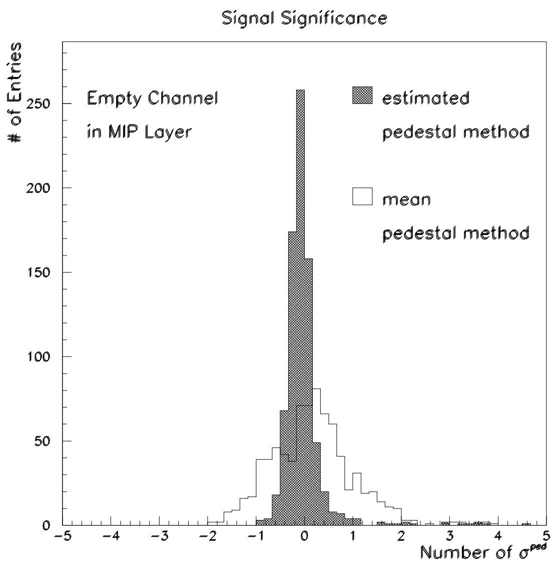

Figure 2.5: **Signal significance in empty channel (MIP Layer). Hatched histogram is for $\hat{S_i}$ and unhatched histogram is for S_i.**

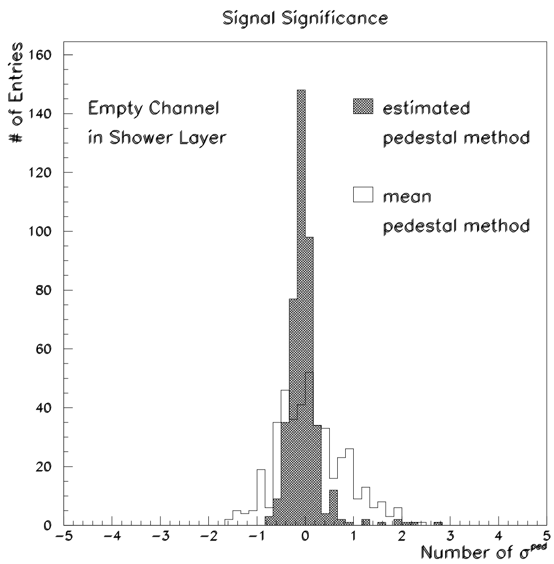

Figure 2.6: **Signal significance in empty channel (Shower Layer). Hatched histogram is for $\hat{S_i}$ and unhatched histogram is for S_i.**

Special care has been taken in identifying empty channels, specially in the layers behind the lead converter. The criteria for identification of an empty channel are:

- location be at least ± 6 strips away from the peak in a layer.
- noise-subtracted ADC counts compatible with mean pedestal at 2σ:

Fig. 2.5 (MIP Layer) and Fig. 2.6 (Shower Layer) show the signal significance of empty channels calculated as described in **method 3**. The hatched histogram shows the signal significance calculated using the estimated pedestal method ($\hat{\mathrm{S}}_\mathrm{i}$) while the unhatched histogram shows the same calculated using the classical method S_i. As can be seen from the width of these two distributions, the accidental rate of an empty channel being identified as a signal channel is significantly greater in the case of the classical method than in the estimated pedestal method. $\hat{\mathrm{S}}_\mathrm{i}$ has a very narrow distribution going upto only $\pm 1\ \sigma^{ped}$, while S_i has a broader distribution going upto $\pm 2\ \sigma^{ped}$. Hence the use of the estimated pedestal method helps in correctly identifying the empty channels by accounting for correlation between channels.

The test of the pedestal subtraction method comes from a comparision of the pedestal calculated from the data with the real pedestal distribution obtained from a pedestal run.

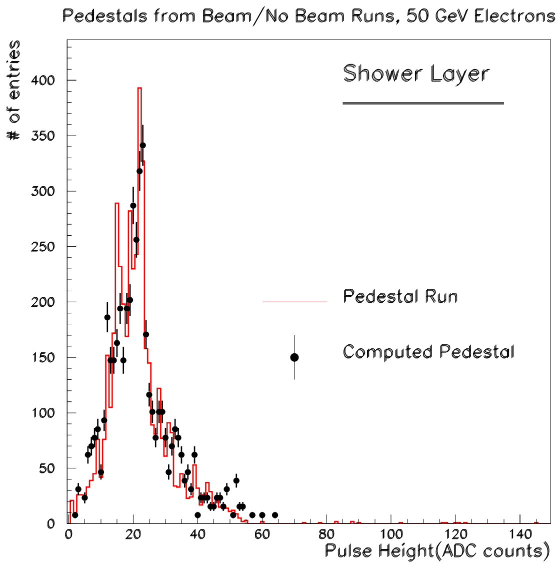

Figure 2.7: **Pedestal computed from data compared to real pedestal distribution for 50 GeV electrons in a layer behind the converter.**

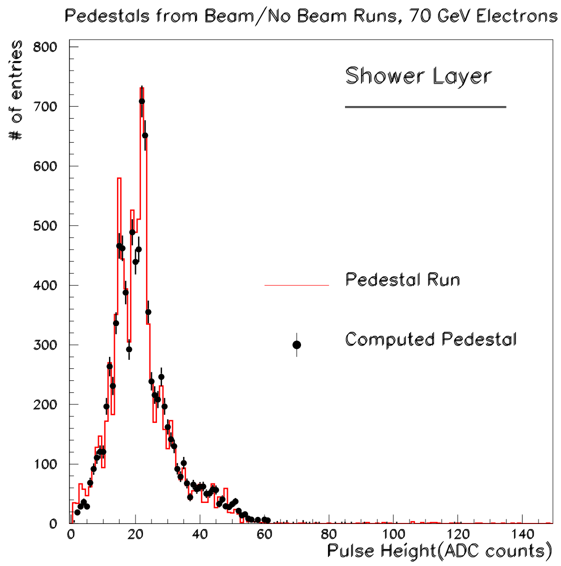

Figure 2.8: **Pedestal computed from data compared to real pedestal distribution for 70 GeV electrons in a layer behind the converter.**

- **Shower Layers:** Fig. 2.7 (50 GeV) and Fig. 2.8 (70 GeV) shows a comparision of the pedestal computed from data to the real pedestal distribution for a given channel in a layer behind the converter. For shape comparision, the distribution obtained from data were normalized to that from pedestal runs by the number of events. Note the reasonable agreement in shape. The means and sigmas of these two distributions differ by a maximum of 2 ADC counts for both 50 and 70GeV electrons. The ratio of these distributions are shown in Fig. 2.9 for both 50 and 70 GeV electrons. The ratios are within 0.5σ of each other. We quote an error of 2 ADC counts in maximum from pedestal subtraction in the shower layers for both 50 and 70 GeV samples. This also shows that pedestal subtraction has been done correctly in the layers behind the converter. This enters as a systematic error in the electron showers.

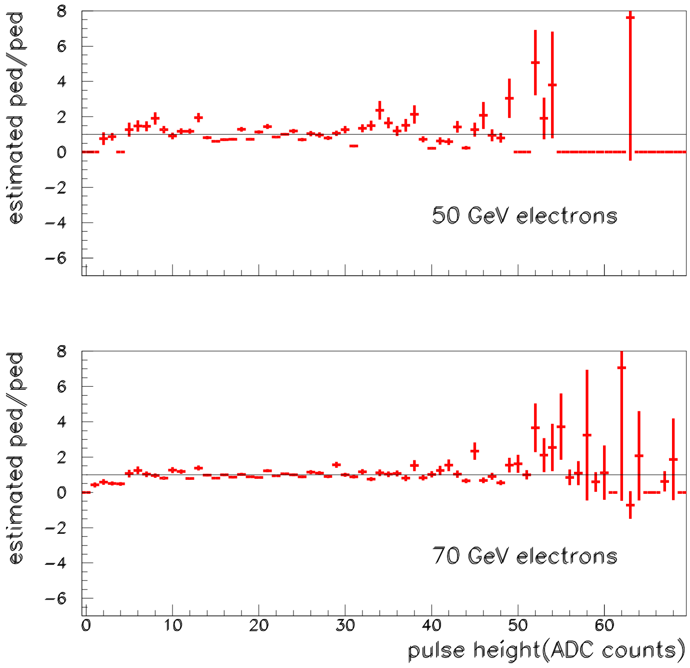

Figure 2.9: **Ratio of estimated pedestal from beam run and real pedestal, for shower layer channels, for 50 and 70 GeV electrons respectively.**

- **MIP Layers:** Unfortunately, for the MIP layers the pedestal settings changed between the data run at 50 GeV and the pedestal run. This resulted in a difference of about 10 ADC counts between the pedestal mean computed from the data and that from the actual pedestal run. This will contribute an error both to the determination of the MIP signal and to the characterization of the electron shower (described later). Fortunately for the electrons at 70 GeV there was no such discrepancy, the difference in mean being 1-2 ADC counts.

Eventually, Fig. 2.10 shows the MIP and Shower distribution of an electron event at 70 GeV in ADC counts before and after pedestal subtraction.

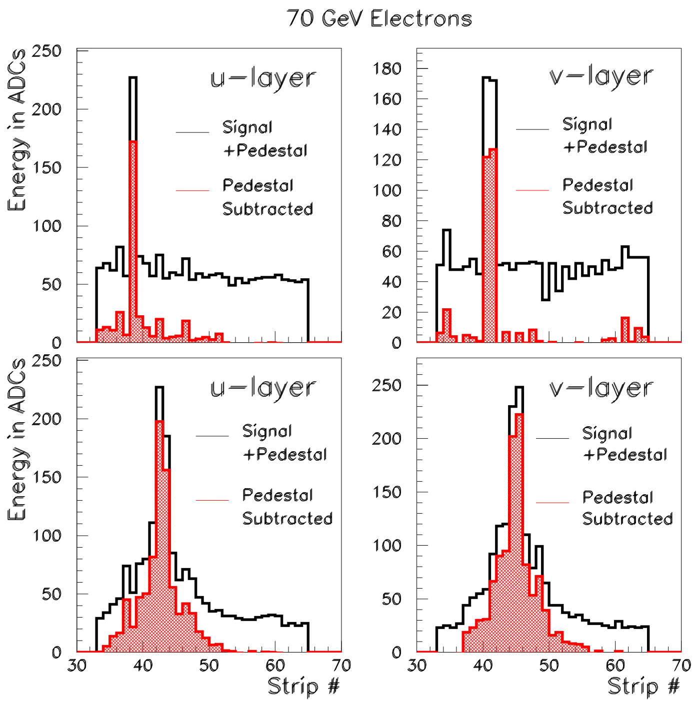

Figure 2.10: **Signal in ADC counts before and after pedestal subtraction in all layers of FPS for a selected event. Top plots show signal in MIP layer, bottom plots show the showers.**

2.3 The Final sample of Electrons

The selection algorithm described previously has been applied to electron samples taken at three different energies of 30, 50 and 70 GeV. Out of 5494 events taken at 30 GeV, none passes the selection criteria. At 50 GeV, out of 2855 events, only 46 were selected and at 70 GeV, 97 out of 10,819 were selected.

At this point, since we do not have an absolute scale for the detector, the energy in the shower layers were normalized to the energy deposited by the particle in the MIP layers. The sum of the energy deposited in an adjacent pair of strips in the front layers by an electron, computed on an event by event basis was used to characterize the MIP signal. The mean value of the MIP distribution is then taken as the energy deposited by a minimum ionising track and its RMS width divided by sqrt(numberofevents) is taken as the error on the MIP. The global definition of a MIP is then the average of the energy deposited in both U- and V- layers:

$$\mathrm{MIP} = \frac{\mathrm{MIP(ULayer)} + \mathrm{MIP(VLayer)}}{2}$$

The MIP value is 152.5 ± 6.8 (150.0 ± 5.6) ADC counts for 50 GeV (70 GeV) electrons, close to the results found from pions runs (≈ 155 –see section 4). Hence, the unit of energy of an electron shower is MIPs. Charge division factors for chips in the shower layers have been taken into account in this conversion, according to the numbers quoted in table 2. Fig. 2.11 shows the MIP distribution in ADC counts for selected electron events at 50 and 70 GeV respectively.

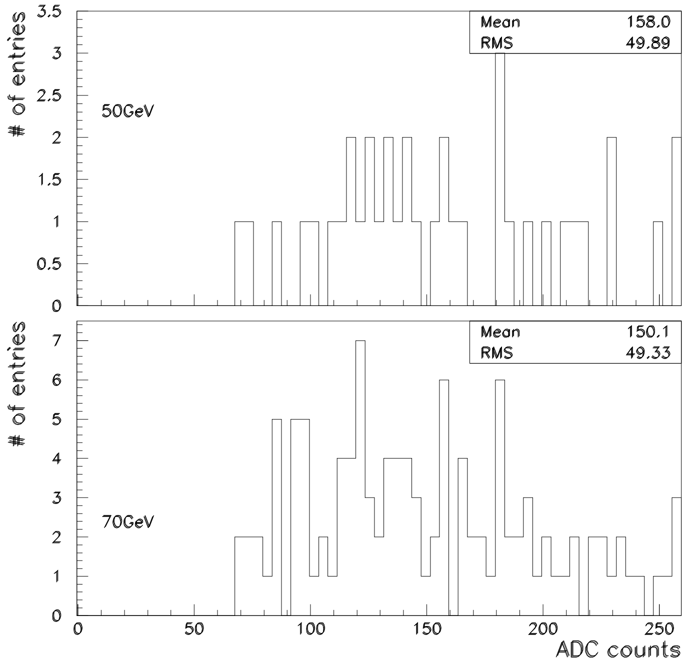

Figure 2.11: **MIP distribution in ADC counts for the selected events at 50 and 70 GeV. Signal is pedestal subtracted.**

A visual scan of the selected events at all energies show the presence of low energy particles in the sample which deposit very small amounts of energy in the layers behind the lead converter.

This may be due to the presence of pions in the electron beam. In order to remove these low energy particles (pions), apart from the selection criteria already described, it is further required that:

- peak of the shower profile in both the downstream layers should be greater than 5 MIPs.
- the three central strips of the shower profile in both the layers should have $\geq 50\%$ of the total energy of the shower.

These additional criteria removed the low energy contamination and only 22 events survived at 50 GeV, while at 70 GeV, 35 events survived.

Fig. 2.12 shows the electron shower profile in MIPs at 50 GeV after pedestal subtraction. The distribution is centered around the position of the peak strip. The error bars are statistical, while the band shows the dominant systematic error on the shower (described later). The RMS width of the shower in the U Layer is 3.9 strips, while in the V Layer, it is 4.0 strips. The peak strip has 16.2 (14.5) MIPs in the U Layer (V Layer).

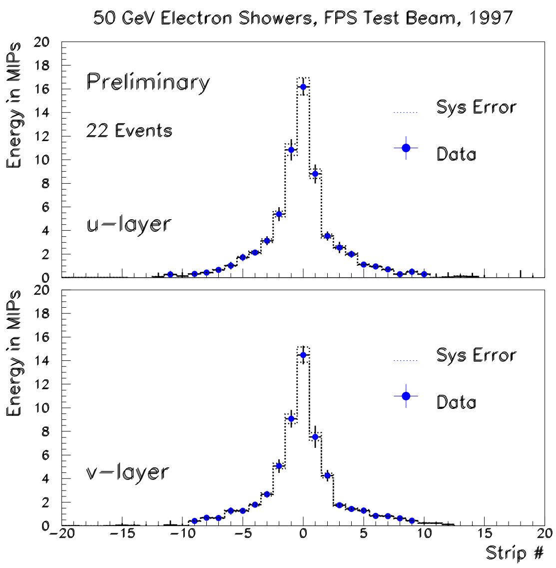

Figure 2.12: **Electron shower in MIPs at 50 GeV. Top plot shows profile in U Layer and the bottom shows the V Layer.**

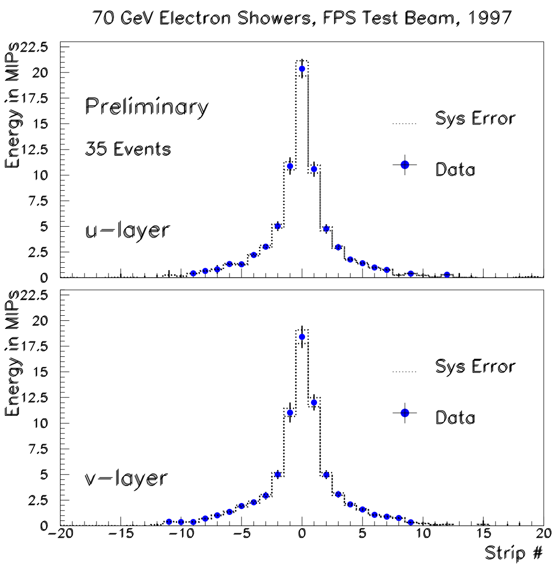

Figure 2.13: **Electron shower in MIPs at 70 GeV. Top plot shows profile in U Layer and the bottom shows the V Layer.**

Fig. 2.13 shows the shower profile for 70 GeV electrons. The RMS widths of these distributions are 3.5 and 4 strips for the U and V Layers, respectively. The peak strip has 20.4 (18.4) MIPs in the U Layer (V Layer).

The integrated shower profiles for 50 and 70 GeV electrons are compared to each other in Fig. 2.14. The top plot shows the comparision in U Layer, while the bottom shows the comparision in V Layer. The data does not show an evolution of the shape of the profile with energy, the profile for 70 GeV electrons has the same width as that of the 50 GeV electrons in both the layers. In the case of 50 GeV electrons, the central strip has $25.9\% \pm 10.8\%(25.9\% \pm 11.8\%)$ in the U Layer (V Layer) and for 70 GeV, the central strip has $28.9\% \pm 11.5\%(25.4\% \pm 12.2\%)$ in the U Layer (V Layer).
The data however, shows increase in total energy deposited in the shower layers with beam energy. The mean total energy deposited in the shower layers are 61.25 ± 15.25 and 55.68 ± 16.7 MIPs for U and V Layers respectively for 50 GeV electrons, while for 70 GeV they are 69.17 ± 25.98 and 72.1 ± 25.89 MIPs.

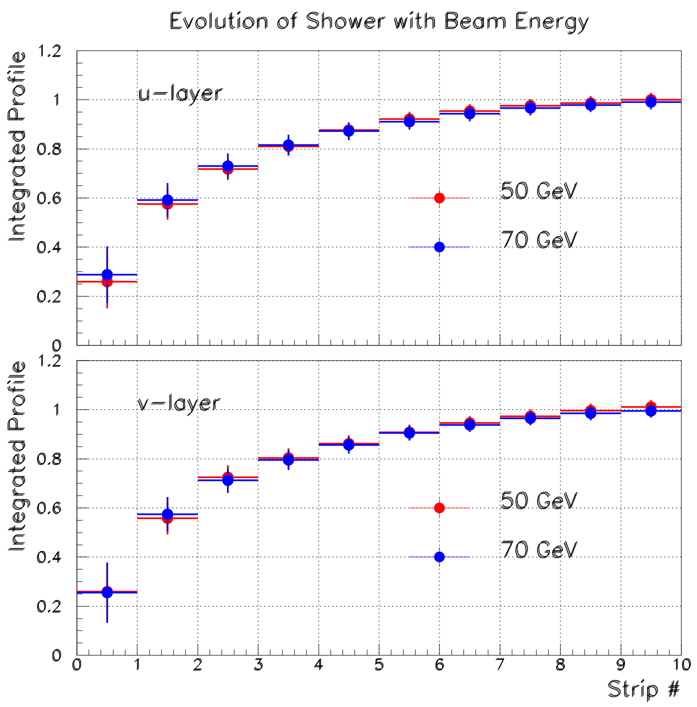

Figure 2.14: **Comparision of integrated shower pfile at 50 and 70 GeV.**

2.4 Systematic Studies

The main sources of error in the electron studies come from pedestal subtraction and the determination of the MIP signal. These constitute three different types of error that can affect the electron showers:

- The 2 ADC count error we assign from pedestal subtraction in layers behind the converter. The effect of this error on the shower profile is shown in Fig. 2.15 and 2.16 for 50 and 70 GeV electrons respectively. As can be seen, this error is ±0.18MIPs (±0.15MIPs) in U (V) Layer for 50 GeV electrons and for 70 GeV electrons, it is ±0.21MIPs±0.17MIPs) in U (V) Layer.

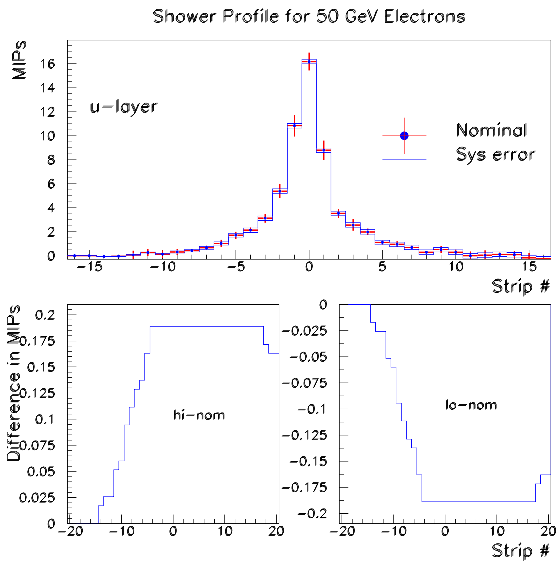

Figure 2.15: **Effect of error of pedestal subtraction in shower layer on shower profile at 50 GeV.**

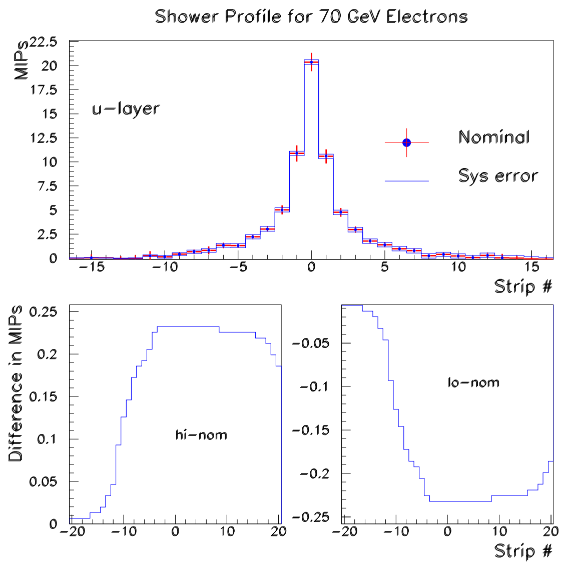

Figure 2.16: **Effect of error of pedestal subtraction in shower layer on shower profile at 70 GeV.**

- since the shower profiles are normalized by the MIP signal in the layers in front, any error in MIP calculation will automatically transform into an error in the shower. As described earlier, the error that comes from pedestal subtraction in the MIP layer, is minimal for 70 GeV electrons, however, for 50 GeV electrons this error is a discrepency of 10 ADC counts in MIP determination. The effect of this error is a fractional change in the total energy in the shower profile by ∼1.8 MIPs in both the layers. Secondly, the finite RMS width of the MIP distribution will also contribute to the uncertainty in electron showers. This is by far the largest source of systematic error in the shower profiles. Its effect is shown by the band in Fig. 2.12 and 2.13. This gives an error in the peak value by ±0.7 (±0.65) MIPs in the U (V) Layer for 50 GeV electrons, while for 70 GeV electrons, the peak is changed by ±0.4 (±0.5) MIPs in the U (V) Layer.

Compared to the statistical errors on the shower profiles, the systematic errors are smaller but not negligible.

3 Comparison data vs Monte-Carlo

The selected events have been compared to simulated electrons tracks in order to test the reliability of the Monte Carlo.
For this purpose, electrons have been generated using ISAJET [3] at 30 GeV, 50 GeV and 70 GeV with a polar angle of $\theta = 15^0$ mimicking the FPS modules orientation. Similar geometry and configuration have been adopted in GEANT for both module types. Eventually generated samples have been processed through this Upgrade version of GEANT.

3.1 Total energy deposition in the shower layers

The total energy deposited in the shower layers by 50 and 70 GeV electrons are displayed in figures 3.17 and 3.18 where they are compared to Monte Carlo distributions. The corresponding values, expressed in MIPs, are reported below for both samples.

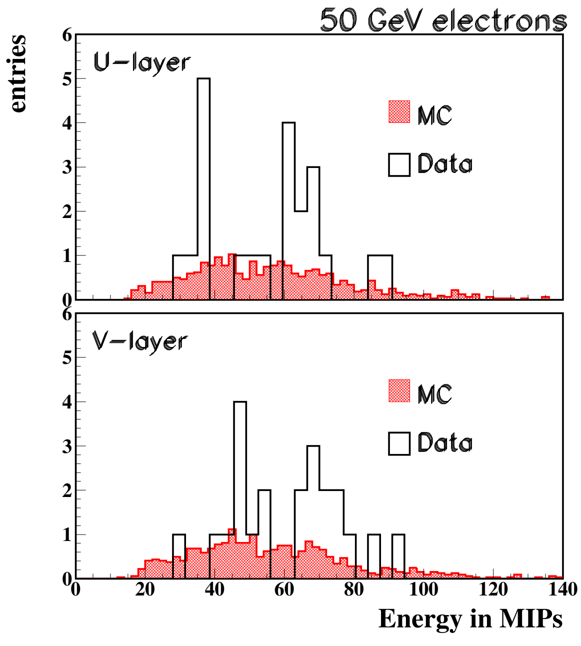

Figure 3.17: **Total energy deposited by 50 GeV electrons in both U- and V- layers (shower layers)**

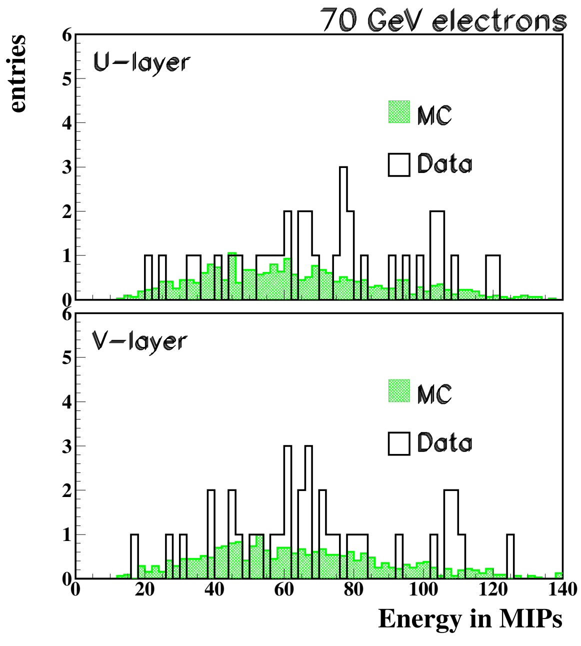

Figure 3.18: **Total energy deposited by 70 GeV electrons in both U- and V- layers (shower layers)**

Despite the limited statistics and the broadness of the distributions, the average values as well as the width of the distributions appear in good agreement:

$$
\begin{array}{lll}
\mathrm{E}^{\mathrm{U}}_{\mathrm{TOT}}(50\ \mathrm{GeV}) & \mathrm{Data}: 56 \pm 18\ \mathrm{mip} & \mathrm{MC}: 56 \pm 22\ \mathrm{mip} \\
\mathrm{E}^{\mathrm{V}}_{\mathrm{TOT}}(50\ \mathrm{GeV}) & \mathrm{Data}: 61 \pm 17\ \mathrm{mip} & \mathrm{MC}: 56 \pm 23\ \mathrm{mip} \\
\mathrm{E}^{\mathrm{U}}_{\mathrm{TOT}}(70\ \mathrm{GeV}) & \mathrm{Data}: 72 \pm 26\ \mathrm{mip} & \mathrm{MC}: 64 \pm 26\ \mathrm{mip} \\
\mathrm{E}^{\mathrm{V}}_{\mathrm{TOT}}(70\ \mathrm{GeV}) & \mathrm{Data}: 69 \pm 22\ \mathrm{mip} & \mathrm{MC}: 64 \pm 26\ \mathrm{mip}
\end{array}
$$

where the error represents width (68% prob.). The comparison data vs MC show a discrepancy below 9% in the average values at 50 GeV, while the difference reaches 11% at 70 GeV. The dependence of the energy deposited with the beam energy will be reviewed in detail in a following section.

3.2 Electrons Shower profile

The shower profile of the electrons is compared to Monte Carlo predictions in Fig. 3.19 and 3.20 for both U and V layers. The scales have been converted to MIP units, following the same procedure as explained in the previous section.

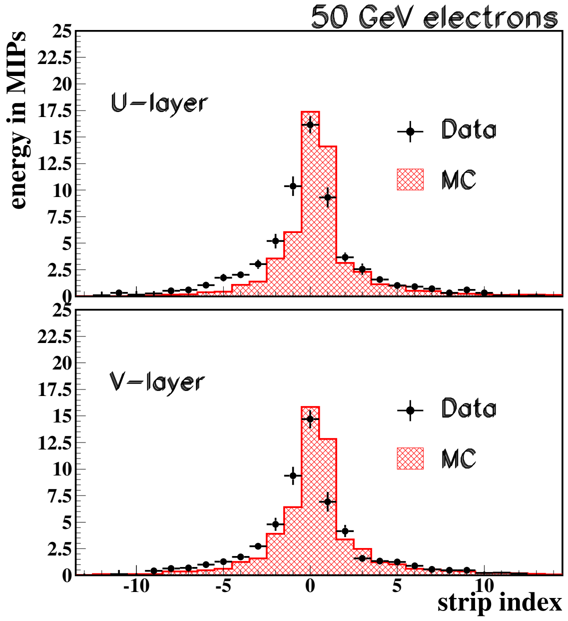

Figure 3.19: **Energy profile deposited by 50 GeV electrons in the U-layer (shower layer)**

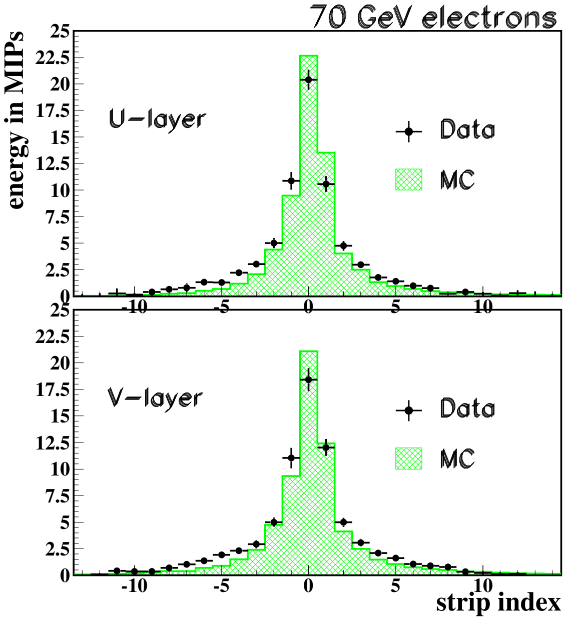

Figure 3.20: **Energy profile deposited by 70 GeV electrons in the U-layer (shower layer)**

In both cases the agreement looks reasonable, although a 1.5σ discrepancy is seen in the central strip in the four cases. The widths of the electron showers are compatible but seem about one strip wider in the data than expected.

Kolmogorov tests have been applied in order to determine the probability that the two distributions come from the same parent distribution. Monte Carlo distributions were considered as the reference (and hence have no associated error) while only statistical uncertainties have been taken into account for the data. It should be noticed that Kolmogorov tests with binned data, as it is the case here, tend to be shifted slightly higher than expected (by around 5%) [4]. Therefore the following numbers have to be considered carefully and seen as an indication of the compatibility of the distributions.
For 50 GeV candidates, a compatibility of 33% for the U- layer distributions (21% for shape alone and 56% for normalisation) and 58% for the V- layer (26% for shape and 91% for normalisation) is found. Clearly here the discrepancy comes from the left side of the distribution which is more symmetric in the data than it appears in the MC sample.
Regarding 70 GeV events, higher probabilities of 85% and 86% are found for U- and V- layers. Here both MC and data are in good agreement in the shape as well as in the global normalisation.

More generally, it should be noted here that the Monte Carlo distributions show a significant asymmetry in the energy distribution whereas data do not. The source of the discrepancy –if not of statistical source– has still to be cleared up. The presence of an extra space between modules in the TB configuration that has not be simulated in the Monte Carlo may be the source of this problem.

3.3 Electrons integrated energy profile

The integrated energy profiles for the first 10 strips aside the central strip are shown in the Fig. 3.21 and 3.22.

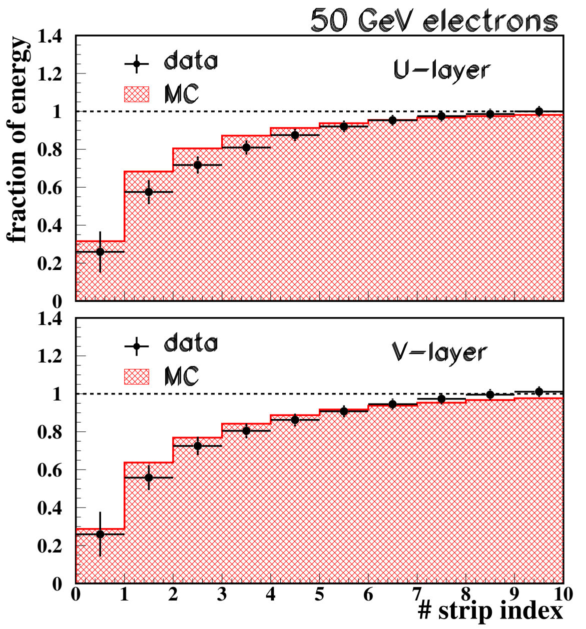

Figure 3.21: **Integrated energy profile of 50 GeV electrons in the U-layer (shower layer)**

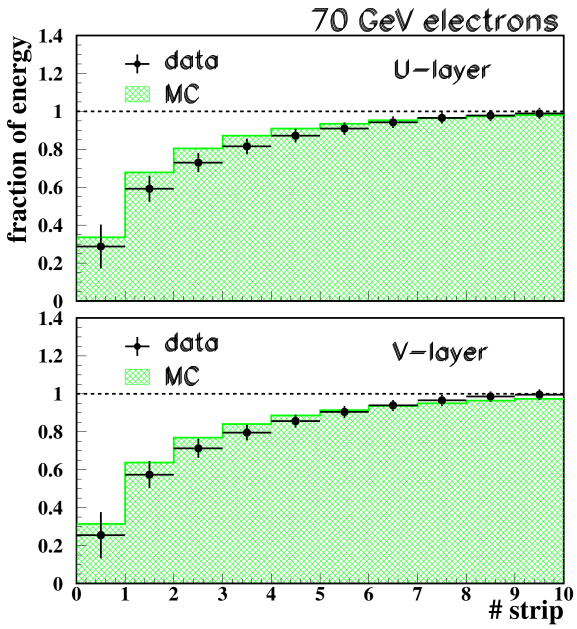

Figure 3.22: **Integrated energy profile of 70 GeV electrons in the U-layer (shower layer)**

The data match reasonably the expectations, although a small discrepancy is measured in the three central strips. However, results show a good compatibility with the simulations, given the level of statistical uncertainties quoted for the data sample.

3.4 Dependence in the beam energy

A comparison between data and Monte Carlo has been performed. We observe that:

- the width of the shower profile seems not to be affected significantly as beam goes up from 50 to 70 GeV. This behaviour is confirmed by the MC samples, where no changes are seen among the two samples. As the beam energy increases from 10 to 200 GeV, no significant difference is observed in the MC (-0.1 strip..)
- the total energy averaged on the both U- and V- layers increases by 18.8% in the data as one goes from 50 to 70 GeV. A change of 12.5% only is seen in the MC (for both U- and

V-). One should note here that for the V- layer alone a 12.3% increase is seen in the data, in remarkabely good agreement with the MC prediction. Fig. 3.23 shows the predictions of the total energy deposited in the shower for different values of the incoming electron energy. The spread is also plotted. The two values in the data are shown in reasonable agreement with the expectations.

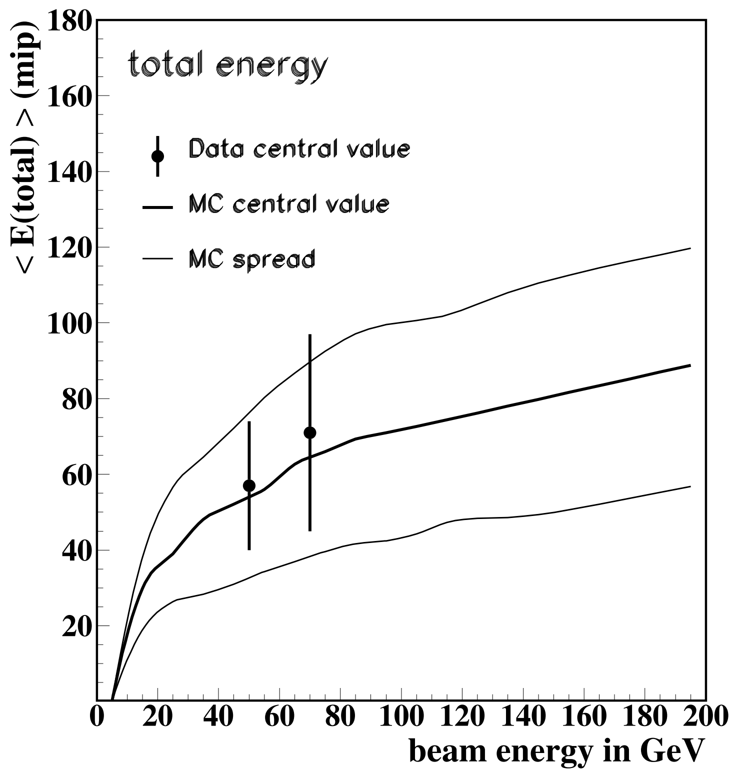

Figure 3.23: **Total energy in mip deposited in the shower layers (u or v) as a function of the energy of the incoming electron. Simulation has been done without any inner detector.**

4 Calibration of the detector

The absolute calibration of the detector has been performed using Minimum Ionizing Particle (MIP) tracks from pions. The two different data sets of pions presented earlier, have been used, allowing two independent measurements of the MIP energy. In the first data set, only one layer was fully equipped and read out, and the accumulated statistics hardly approaches 3K events. The second sample had both the U and V Layers infront of the converter and also the accumulated statistics was high, almost 35K events.

4.1 Pion Run: period 1

Typical ADC spectra obtained in the first layer for pions is shown below: Fig. 4.24 displays signals observed in both an empty channel (no pion) and in a hot channel traversed by a pion, the use of finger counters for triggering providing the a-priori knowledge of the targetted channel. The peak value at 256 ADC counts correspond to the channel ADC saturation.

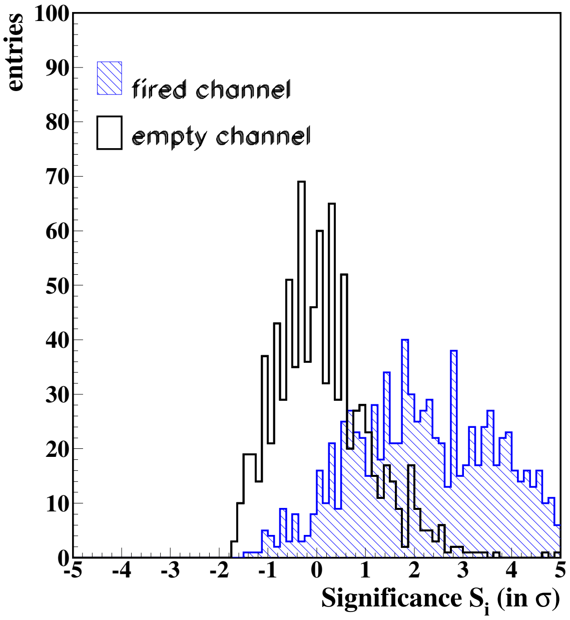

Figure 4.24: **Significances in an empty channel (histogram) and in a hit channel (hatched histogram).**

Pedestal runs were taken for the two different detector configurations. The mean pedestal has a typical value of 35 ADC counts with a width of 25 counts. The distributions were fitted with a gaussian resulting in a reasonnable χ^2, even though better results were obtained from the sum of two independant gaussian distributions.

Signal selection was first done by using **method 1** and then compared to results using **method 2**. It turns out from Fig. 4.26, the significance is drastically increased in the latter case, as correlations between channels in the same layer were taken into account. Using the latter technique, almost no noise is left for a significance of 2σ while keeping high efficiency as we will see later. The use of **method 2** is clearly justified by Fig. 4.25 where the corrected pedestal $\hat{\mathrm{Ped}}_i$ is compared on an event by event basis to the true pedestal distribution: the correspondence is rather good, showing the coherent nature of the noise.
Signal significance obtained from the two methods are compared for both methods in figure4.26 for a typical empty channel.

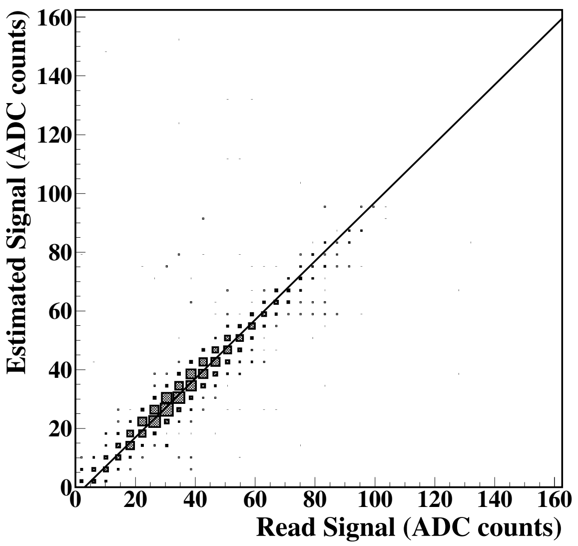

Figure 4.25: **Correlation between the signal readout from an empty channel and the estimated pedestal computed by applying the definition 3 in the text.**

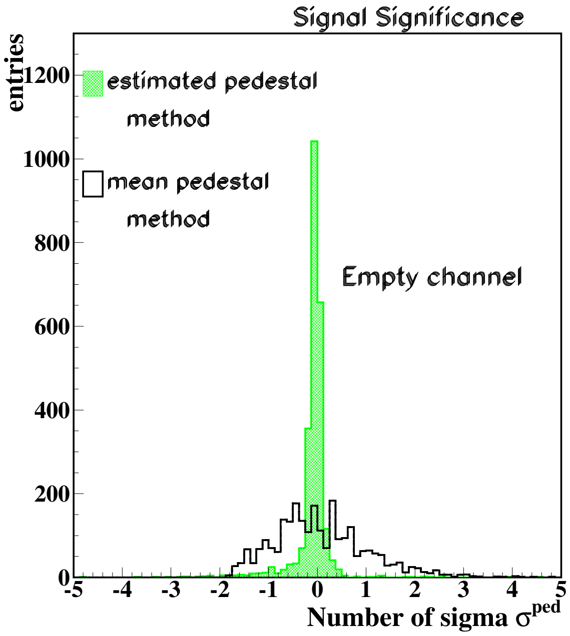

Figure 4.26: **Signal significance as a function of the number of sigmas, as computed from the two methods.**

This outcome translates into the noise rate calculation which shows an increase by a factor 3 of the rejection factor, depending on the requirement put on the significance (see Fig. 4.27). A better efficiency in the hot channel is also achieved as a result of the decreased contribution from noise.

Thus, a requirement of 1.5σ significance leads to an improved efficiency on the signal by about 20% with a value reaching 85%.

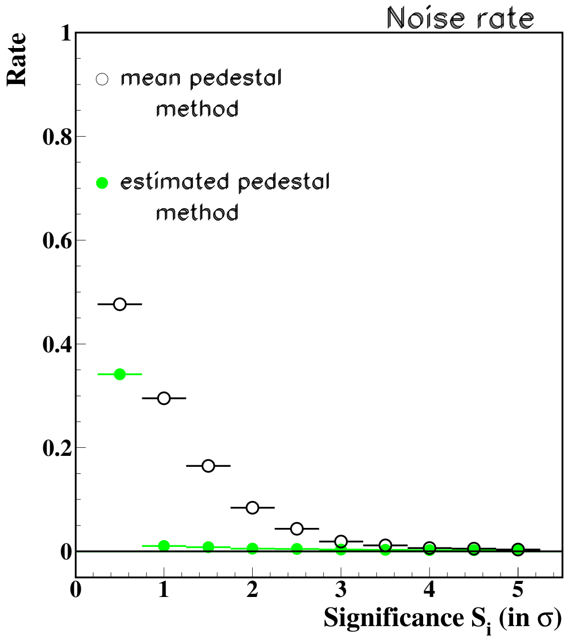

Figure 4.27: **Noise rate as a function of the signal significance in number of sigma for the two definition of S_i.**

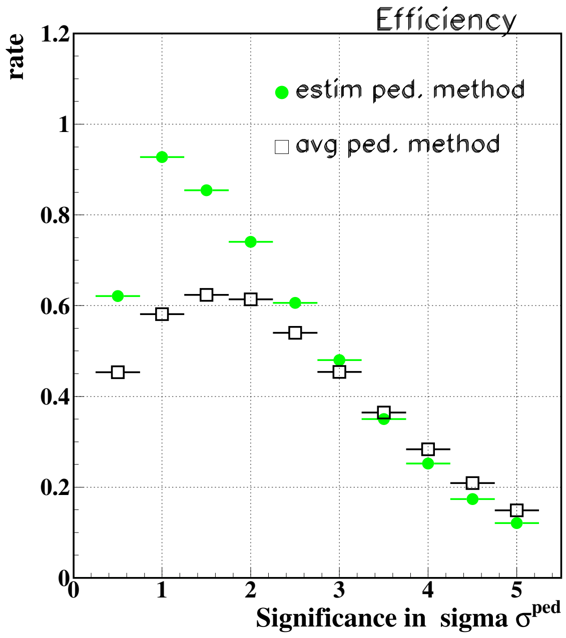

Figure 4.28: **Signal efficiency estimated in a hot channel as a function of the significance, for the two methods.**

A fit of the MIP signal has been performed from the 32 output channels readout from the first layer. Two adjacent strips are hit by the pion beam, as expected from the triangular structure of the nested pairs. In each of the channels noise has been computed for a signal significance of $S_i \geq 2\sigma_i^{ped}$, the latter being calculated using the estimated pedestal technique. Noise subtracted signals are shown in Fig. 4.29. For both of the strips forming the nested pair, an 'efficiency' of 78% was obtained for the signal, whereas, the noise contamination is estimated below 2%.

The sum of the two (noise subtracted-) strips provides the total charge induced by the crossing of a pion. The observed signal is shown in figure 4.30. The total collected charge is 26 fC. This result will be expressed in term of photoelectrons in the next section.

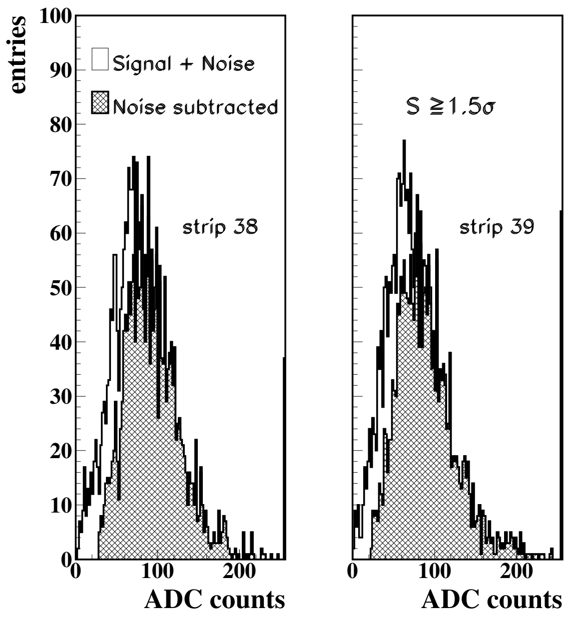

Figure 4.29: **Distribution of the two adjacent strips hit by pions. The hatched histogram correspond to the noise subtracted signal with a significance of 1.5 sigma.**

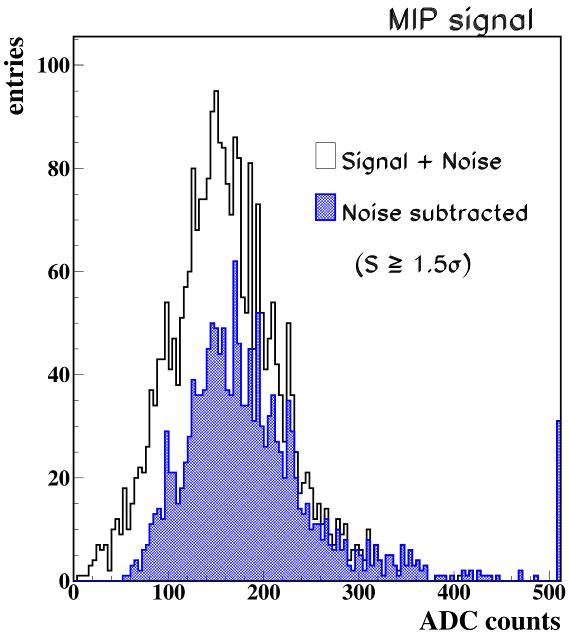

Figure 4.30: **Distribution of the signal seen as the sum of the two adjacent strips. The hatched histogram correspond to the noise subtracted signal with a significance of 1.5 sigma.**

4.2 Pion Run: period 2

For the latter period of the pion runs, all four layers of the detector were equipped and readout, however, the finger counter was not used. But, compared to the electron beam, the pion beam had a narrower spread, so it was relatively easier to identify empty channels for pedestal subtraction.

A simple selection algorithm was used to select pion events:

- only two adjacent strips are hit in the MIP layers.
- there should be only one and only one hit in each MIP layer.
- peak in each layer should be $> 3\sigma$ of the pedestal mean.

Pedestal subtraction for these pion runs were done by using **method 2** after proper identification of empty channels by requiring the pulse height to be $< 2\sigma$ of the pedestal mean. The MIP in each layer was calculated as the sum of the ADC counts in an adjacent pair of strips.

After pedestal subtraction, it was further required that the signal significance be greater than 1.5σ.

Fig. 4.31 shows the MIP distribuion in the U Layer from this sample at a signal significance of 1.5σ. The distribution gives a mean of 158.1 with an RMS of 53.94.

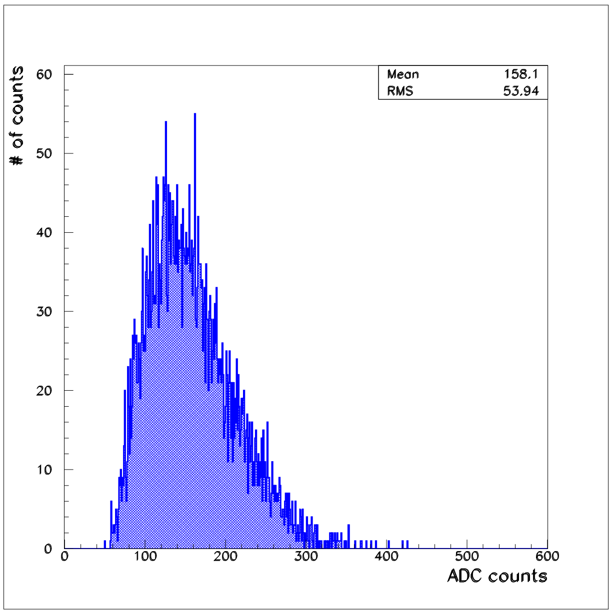

Figure 4.31: **MIP signal in U Layer with signal significance of 1.5σ.**

The VLPC cassette used for these runs had a gain of 2.26 fC of charge per photoelectron. At a temperature of 6.5K and a bias voltage of 6.7V, the cassette had a full gain of 14,100 photoelectrons at full scale. The MIP signal has a mean of 158.1 ADC counts and the full scale is 40 fC or 256 ADC counts, which gives:

$$158.1 \text{ ADC/MIP} \; * \; (40 \text{ fC}/256 \text{ ADC}) \; = \; 24.7 \text{ fC/MIP}$$

$$\rightarrow (24.7 \text{ fC/MIP})/(2.26\text{fC/photoelectron}) \; \approx 11 \text{ photoelectrons/MIP}$$

From the RMS width of the MIP distribution, we get an error of +/-2 photoelectrons per MIP. The measurement from the low statistics run taken during the begining of the data taking period gives a total charge of 26 fC/MIP which translates into 11.5 photoelectrons/MIP. Ofcourse, the temparature dependence of the VLPC gain, effect of the asymmetry of the MIP distribution has to be folded into the error. Also, the MIP distribution in the V Layer is not understood completely, hence, it is not included in the results so far. Further work underway should finalise the systematics and the understanding of the MIP distribution in the V Layer.

5 Conclusion

During this test beam two modules of the Forward Pre-shower detector have been tested.

During this test beam, the level of electronic (and coherent) noise was a major concern. This made mandatory the development of pedestal subtraction techniques based on the determination of the coherent part of the noise. Several methods have been used and cross-checked.

From the physics point of view, the main motivation was the characterization of the energy of the showers generated by electrons traversing the lead converter. We achieved to measure the width and the total energy of these depositions for 50 GeV and 70 GeV electron beams. Comparisons with MC simulation turned out to be satisfactory, showing a reasonable agreement in the expected shape as well as in the total energy deposited in the detector. Beam energy dependence of the electron showers has also been investigated and compared to expected values from simulation. Results are shown to be consistent with each other.

The second point was the absolute calibration of the detector. To achieve this, high statistics charged pions samples have been used. Pions tend to deposit a MIP in the layers in front of the converter. By measuring the corresponding amount of collected charge we found 11 ± 2 photoelectrons per MIP in a nested pair of strips. This number is preliminary and the quoted error has been increased to account for uncertainty in the temperature dependence of the VLPC gain.

A Readout specification: dynamical range

During the first period, the two front layers were equiped with output cables, allowing 32×2 channels to be readout through the chips A0 and A1 for the U-layer and E0 and E1 for the V-layer. The dynamical range for all chips was set at 100 fC.
Most of the statistics has been accumulated during the period 2. All the four layers were equipped with VLPC readout, readout via 8 chips, whose dynamical range settings were varied from run to run as reported in Table 2. Chips F2 and F3 were used for the front U layer and 92 and 93 for the front V. For the layers behind the lead, chips E0 and E1 were used for the U and A0 and A1 for the V layer.

Run number	A0/A1 Layer 4	E0/E1 Layer 3	92/93 Layer 2	F2/F3 Layer 1
4098-4113	150 fC($\times 1/4$)	150 fC($\times 1/8$)	60 fC	60 fC
4114-4131	150 fC($\times 1/4$)	90 fC($\times 1/8$)	50 fC	50 fC
4132-4141	90 fC($\times 1/4$)	90 fC($\times 1/8$)	50 fC	50 fC
4142-4187	150 fC($\times 1/4$)	90 fC($\times 1/8$)	40 fC	40 fC

Table 2: Full dynamical range of the readout channels for the 8 chips. The charge division factor is also indicated.

B Pedestal subtraction techniques

The use of efficient procedures of pedestal subtraction turned out to be the key point in the analysis of the Test Beam data. As an illustration of the problems we faced, Figure B.32 shows a typical pedestal distribution compared to a channel hit by pions during a beam run. Figure B.33 displays the correlation between two individual channels in a pedestal run.

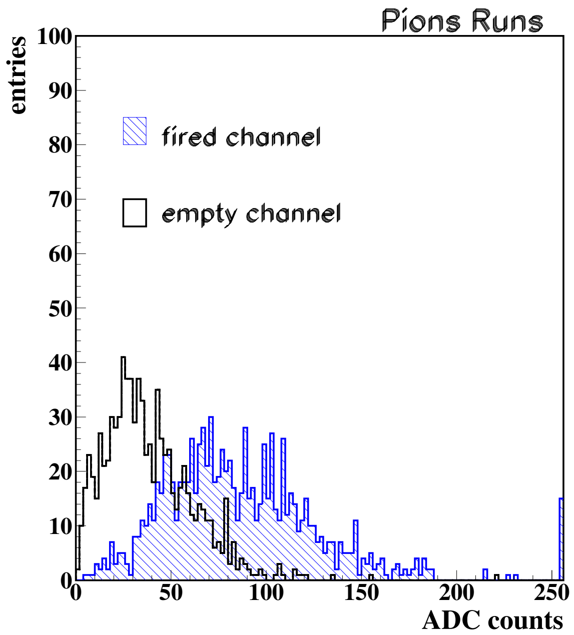

Figure B.32: **ADC counts distributions in a bonded channel (histogram) and in an unbonded channel (hatched histogramm).**

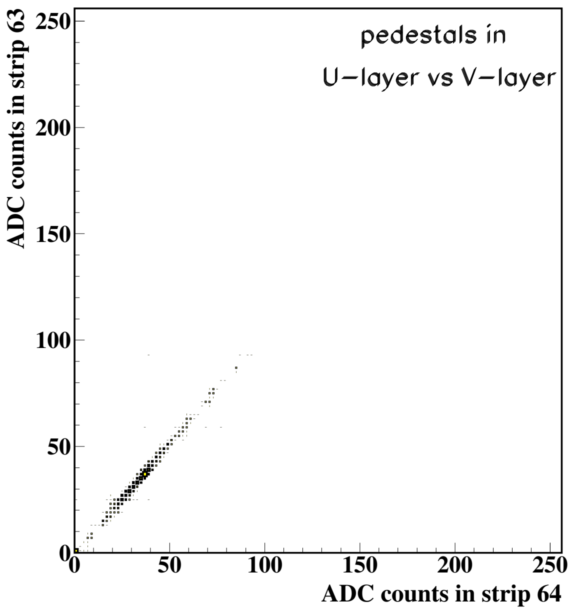

Figure B.33: **ADC counts distributions for two bonded channels during a typical pedestal run. The two channels belong to different layers.**

From these two examples, it can be seen that:

- the noise spectrum covers almost one third of the total dynamic range of the channel, reducing the sensitivity for signal extraction.
- the noise distribution is far from behave as a gaussian, making inadequate the use of traditional methods relying on mean and width values calculated from a single "gaussian-like" fit of the pedestal.
- there is strong positive correlation (Fig. B.33) between individual channels, showing the presence of substantial coherent noise in the setup or in the experimental hall.

Several alternate methods have been developed to deal with these problems. Among them three have been extensively used:
In the first one, pedestal ditributions are used to compute the pedestal mean for the run, which is to be subtracted for every channel in every event (**method 1**). However, in this way one ignores the channel to channel correlations arising from coherent noise.
In order to account for these effects, correlation coefficients are computed from the *pedestal runs*, while empty channels in *beam runs* are used to provide for the absolute value of the noise, on an event by event basis. This technique requires the identification of empty channels during data taking. **Method 2** has been used on the earlier pions data where fired chanels were known a priori. In the case the position of the empty channels were not known, **method 1** was used to find struck strips and **method 2** was applied on the resulting sets of chanels to account for correlations (**method 3**).

B.1 Method 1: "Mean pedestal" subtraction

The detection of an energy deposition in a given channel "i" is based on its signal significance S_i defined as:

$$\mathrm{S_i} \equiv \frac{\mathrm{ADC_i} - <\mathrm{Ped_i}>}{\sigma_{\mathrm{i}}^{\mathrm{ped}}}$$

where $\mathrm{ADC_i}$ is the number of ADC counts and $<\mathrm{Ped_i}>$ and $\sigma_{\mathrm{i}}^{\mathrm{ped}}$ the pedestal and width computed for the run for that particular "$\mathrm{i^{th}}$" channel. The signal significance, expressed in numbers of standard deviation, is then computed event by event for every channel. We can then determine the noise rejection and thereby the "purity" of the signal in the "$\mathrm{i^{th}}$" channel as a function of significance values.

This is considered as the "classical" method of subtracting pedestal. It is based on pedestal runs and assumes that the fitted distributions are "gaussian-like", giving reliable mean and width values. It should be noted that requiring each signal to be above $\mathrm{S_i} \geq 1\sigma$ is known as "zero-suppression", and is actually used during data taking. However in standard data analysis, signal extraction usually requires a 3σ significance.
A major drawback of this procedure is that correlations between distinct channels are simply ignored.

B.2 Method 2: Technique of the "estimated pedestal"using data

This procedure is well described in [5]. It allows us to account for the coherent contributions of noise, by using the information carried by the empty channels in the data runs.

If the noise affecting a set of channels comes from a common source, then it makes the response of a group of channels to shift up or down together. As an outcome, the ADC counts of two individual counters will be correlated, as shown in Figure B.33. In order to include this information into the pedestal subtraction for the "i^{th}" channel, one has to substitute the former pedestal mean value $< \mathrm{Ped_i} >$ by the quantity $\hat{\mathrm{Ped}}_\mathrm{i}$, defined as:

$$\hat{\mathrm{Ped}}_\mathrm{i} \equiv < \mathrm{Ped_i} > + \frac{\sigma_\mathrm{i}^{\mathrm{ped}}}{\mathrm{N}} \sum_{\mathrm{j=1}}^{\mathrm{N}} \frac{\mathrm{ADC_j} - < \mathrm{Ped_j} >}{\sigma_\mathrm{j}^{\mathrm{ped}}}$$

where the sum runs over all the "N" empty channels. This quantity is thus determined on an event by event basis as the sum of the former pedestal mean $< \mathrm{Ped_i} >$ plus a quantity proportional to the average significance computed over the "N" (other) empty channels *in the data*. In case of substantial common noise between channels, the distribution of $\hat{\mathrm{Ped}}_\mathrm{i}$ will reproduce the typical ADC spectrum of a pedestal signal.
The signal significance is then estimated via the same formula given previously but now with the corrected pedestal:

$$\mathrm{S_i} \equiv \frac{\mathrm{ADC_i} - \hat{\mathrm{Ped}}_\mathrm{i}}{\sigma_\mathrm{i}^{\mathrm{ped}}}$$

and the same remarks apply for the data analyis: efficiency and noise rejection rates may then be estimated as a function of signal significance $\mathrm{S_i}$.

The major drawback of this method is that it relies on a correct determination of an empty channel a priori. This is of course achieved in the test beam for the earlier pion runs where the strips hit by the beam were known.

B.3 Method 3: "Estimated pedestal" using data when empty channels not known a priori

During the later runs (both electrons and pions) the region of the detector hit by the beam was not known a priori, as the beam spot was as large as the physical size of the active region (no finger counters used). Hence, correct identification of empty channels was problematic, specially in the layers behind the lead converter where the electrons shower and the shower energy is spread over a number of scintillator strips.

First, an "empty channel" is required to be ± 6 scintillator strips away from the peak in a given layer. Then the mean and width of the pedestal distribution of this given channel "i" was used by requiring $\mathrm{ADC_i} - < \mathrm{Ped_i} > \ \leq \ 2\sigma_\mathrm{i}^{\mathrm{ped}}$ (**method 1**) to ascertain whether the channel is indeed empty. If identified as an "empty chanel", the latter is used in the calculation of the estimated pedestal, as described in **method 2**

The estimated pedestal has thus been calculated event by event using the following correlations:

- correlation between channels in the same chip.

- correlation between channels from the same layer.
- correlation between channels from different layers on the same side of the converter.

It should be noticed that correlations between front and rear layers, although non-zero, have not been used in this analysis.

References

[1] "The D0 Upgrade", FERMILAB-FN-641/ D0note 2894

[2] "Technical Design Report of the Forward preshower detector for the D0 upgrade" in preparation.

[3] "ISAJET 7.31 - A Monte Carlo Event Generator for pp, $p\bar{p}$ and e^+e^- collisions" F.E. Paige, S. D. Protopopescu, H. Baer and X. Tata

[4] HBOOK Reference Manual Version 4.22

[5] F. Stichelbaut, DELPHI note 96-18 HERM 2, Feb. 22 1996.